Optics Communications 431 (2019) 167–173

Contents lists available at ScienceDirect

Optics Communications

journal homepage: www.elsevier.com/locate/optcom

Demonstration of horizontal free-space laser communication with the effect of the bandwidth of adaptive optics system

Rui Wang [a,b], Yukun Wang [a], Chengbin Jin [a,b], Xianghui Yin [a,b], Shaoxin Wang [a], Chengliang Yang [a], Zhaoliang Cao [a,*], Quanquan Mu [a], Shijie Gao [c], Li Xuan [a]

[a] State Key Laboratory of Applied Optics, Changchun Institute of Optics, Fine Mechanics and Physics, Chinese Academy of Science, Changchun, Jilin, 130033, China
[b] University of Chinese Academy of Sciences, Beijing, 100049, China
[c] Changchun Institute of Optics, Fine Mechanics and Physics, Chinese Academy of Science, Changchun, Jilin, 130033, China

ARTICLE INFO

Keywords:
Free space laser communication
Adaptive optics
Horizontal turbulence
Bit error rate

ABSTRACT

The performance of free-space laser communication (FSLC) is greatly decreased by horizontal atmospheric turbulence. Adaptive optics is used to overcome horizontal turbulence. This study investigated the effect of the 3 dB bandwidth of an adaptive optics system (AOS) on FSLC performance by using power-in-bucket (PIB) method, which considers the effect of receiving aperture and then, can accurately evaluate of the effect of system bandwidth on the communication performance. A 9 km horizontal maritime link experiment was performed through adaptive correction to validate the theoretical analysis. Results indicate that the effect of system bandwidth can be accurately evaluated using PIB method. This work provides a basis for designing and evaluating AOSs for FSLC.

1. Introduction

Free-space laser communication (FSLC) has been widely studied because of its advantages of high bandwidth, strong ability to resist interception, and anti-interference [1–4]. However, the communication performance of FSLC in earth-to-satellite and horizontal links is greatly decreased due to the effect of atmospheric turbulence [5–9]. To solve this problem, previous studies adopted adaptive optics (AO) technique in FSLC systems and analyzed the effects of adaptive correction on communication bit error rate (BER) [10–15]. Many researchers have also studied the effect of residual aberrations on FSLC performance while different Zernike modes are corrected [16–21]. The influence of the 3 dB bandwidth (f_{3dB}) of AO was also studied with variations in Greenwood frequency (f_G) [22,23]. Kaufmann studied the effect of f_G/f_{3dB} on the performance of coherent communication and used Strehl ratio (SR) to represent the receiving energy efficiency of FSLC to calculate BER [24]. By using this method, Liu et al. performed numerical simulation [25] and Cao et al. conducted validation experiment in laboratory [26].

Previous works used SR to represent the receiving energy efficiency of FSLC but did not consider the influence of the laser-receiving end face area. However, the small size of the end could affect the coupling efficiency (CE) and BER of FSLC. As such, SR method cannot precisely evaluate the receiving energy efficiency. To overcome this shortcoming, our group proposed power-in-the-bucket (PIB) method [27]. In the present study, we aim to establish the relation between PIB and f_G/f_{3dB} and accurately evaluate the effect of the system bandwidth on communication BER. We also conducted an experiment using 9 km maritime laser communication to validate the theoretical model.

2. Analysis of the effect of system bandwidth through PIB method

2.1. CE

The adaptive correction of FSLC is simplified in Fig. 1. A laser beam with initial phase ϕ_0 is distorted by atmospheric turbulence, and distorted wave-front is represented with ϕ. The distortion is corrected by deformable mirror (DM), and residual error is $\phi_r = \phi - \phi'$, where ϕ' is the compensation signal. After the correction, the laser is received by an optical system with entrance pupil diameter D and focal length f, and then coupled into a fiber with cross-sectional radius R. The entrance pupil and focal planes are expressed with the polar coordinates (ρ, θ) and (γ, φ), respectively.

The receiving energy of the fiber should be first obtained to calculate CE. Based on our previous work, receiving energy disturbed by

* Corresponding author.
E-mail addresses: caozlok@ciomp.ac.cn (Z. Cao), muquanquan@ciomp.ac.cn (Q. Mu).

https://doi.org/10.1016/j.optcom.2018.09.038
Received 23 August 2018; Received in revised form 12 September 2018; Accepted 15 September 2018
Available online xxxx
0030-4018/

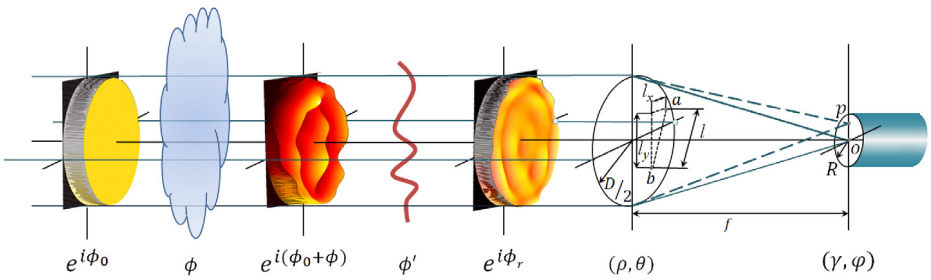

Fig. 1. Diagram of FSLC with adaptive correction.

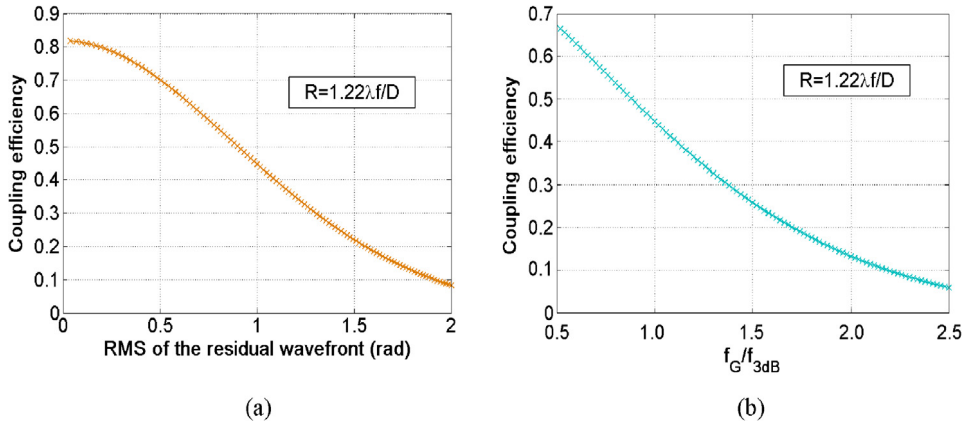

Fig. 2. CE varies with (a) correction error and (b) $f_G/f_{3\mathrm{dB}}$ with$R = 1.22\lambda f/D$.

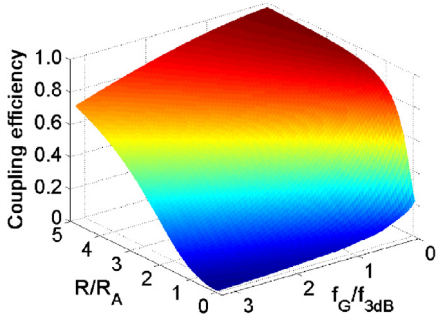

Fig. 3. CE as a function of $f_G/f_{3\mathrm{dB}}$ and R/R_A.

turbulence can be computed accurately with PIB method [27]:

$$\begin{aligned}\langle PIB\rangle &= \zeta\int_0^2\left\langle\int_S \exp\left[i\phi(\rho)\right]\exp^*\left[i\phi(\rho+l)\right]d\rho\right\rangle\times\frac{2RJ_1(\pi Rl)}{l}dl\\ &= \pi^2\left(\frac{AD^2}{4\lambda f^2}\right)^2\int_0^2\left(0.15l^4-0.275l^3-l^2+2l\right)\\ &\quad\cdot\int_{-\infty}^{\infty}\cos\left(\boldsymbol{\Phi}\right)f\left(\boldsymbol{\Phi}\right)d\boldsymbol{\Phi}\times\frac{2RJ_1(\pi Rl)}{l}dl,\end{aligned}\tag{1}$$

where $\boldsymbol{\Phi}=\phi(\rho)-\phi(\rho+l)$, l is the distance between any two points in the pupil area S, A is the amplitude of the incident optical field; λ is the wavelength of the laser, J_1 is the first-order Bessel function, and $f(\boldsymbol{\Phi})$ is the distribution density function of $\boldsymbol{\Phi}$. This function follows the normal distribution, and the expectation is zero. Thus, $f(\boldsymbol{\Phi})$ may be expressed as:

$$f\left(\boldsymbol{\Phi}\right)=\frac{1}{\sqrt{2\pi\left\langle\boldsymbol{\Phi}^2\right\rangle}}\exp\left(-\frac{\boldsymbol{\Phi}^2}{2\left\langle\boldsymbol{\Phi}^2\right\rangle}\right).\tag{2}$$

While the laser transmits through atmospheric turbulence, the variance of ϕ can be determined with Kolmogorov model [28]:

$$\left\langle\boldsymbol{\Phi}^2\right\rangle=\left\langle\left[\phi(\rho)-\phi(\rho+l)\right]^2\right\rangle.\tag{3}$$

For wave-front after the correction, the following equation may be obtained:

$$\boldsymbol{\Phi}_r=\phi_r(\rho)-\phi_r(\rho+l).\tag{4}$$

After substituting $\phi_r=\phi-\phi'$ into Eq. (4), $\boldsymbol{\Phi}_r$ can be rewritten as:

$$\begin{aligned}\boldsymbol{\Phi}_r &= \left[\phi(\rho)-\phi'(\rho)\right]-\left[\phi(\rho+l)-\phi'(\rho+l)\right]\\ &= \left[\phi(\rho)-\phi(\rho+l)\right]-\left[\phi'(\rho)-\phi'(\rho+l)\right]\\ &= \boldsymbol{\Phi}-\boldsymbol{\Phi}'\end{aligned}\tag{5}$$

As $\boldsymbol{\Phi}$ obeys normal distribution and compensation signal $\boldsymbol{\Phi}'$ is conjugated to $\boldsymbol{\Phi}$, $\boldsymbol{\Phi}'$ also obeys normal distribution. According to Eq. (5), $\boldsymbol{\Phi}_r$ also obeys normal distribution. Therefore, the variance of ϕ_r may be written as [29]:

$$\sigma_r^2=\left\langle\boldsymbol{\Phi}_r^2\right\rangle=\left\langle\left[\phi_r(\rho)-\phi_r(\rho+l)\right]^2\right\rangle,\tag{6}$$

where σ_r is the average RMS of ϕ_r (unit is rad).

After the adaptive correction, the receiving energy of FSLC may be expressed as:

$$\begin{aligned}\langle PIB\rangle_r &= \pi^2\zeta\int_0^2\left(0.15l^4-0.275l^3-l^2+2l\right)\times\\ &\quad\left[\int_{-\infty}^{\infty}\cos\left(\boldsymbol{\Phi}_r\right)\frac{1}{\sqrt{\pi\cdot2\sigma_r^2}}\exp\left(-\frac{\boldsymbol{\Phi}_r^2}{2\sigma_r^2}\right)d\boldsymbol{\Phi}_r\right]\\ &\quad\times\frac{2RJ_1(\pi Rl)}{l}dl.\end{aligned}\tag{7}$$

CE is usually computed by:

$$CE=\frac{\langle PIB\rangle_r}{Power_{No\_turb}}=\frac{\langle PIB\rangle_r}{A^2\left(\frac{\pi D^2}{4}\right)},\tag{8}$$

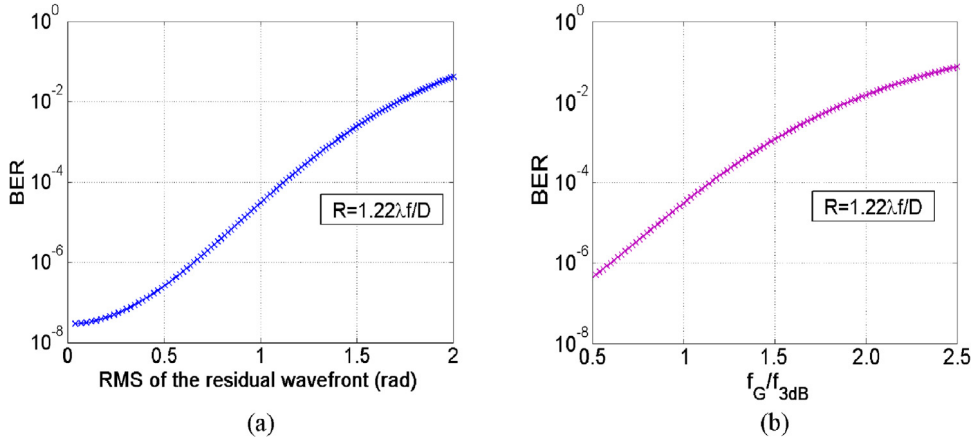

Fig. 4. BER varies with (a) correction error and (b) $f_G/f_{3\mathrm{dB}}$ when $R = 1.22\lambda f/D$.

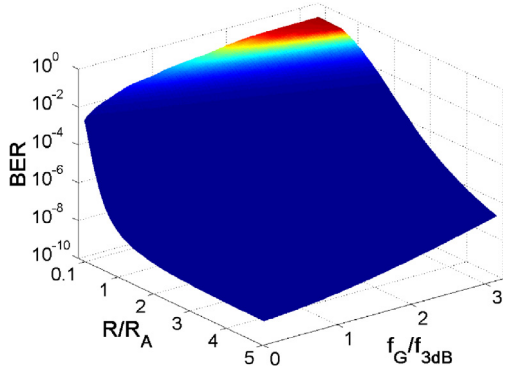

Fig. 5. BER as a function of $f_G/f_{3\mathrm{dB}}$ and R/R_A.

where $Power_{No\_turb}$ represents the total receiving energy without the turbulence effect.

The adaptive correction can be limited by temporal deficiencies, especially for strong turbulence. The bandwidth of the tilt control system is usually high, and the temporal error may be ignored. The present work mainly considers the temporal error caused by the high-order wavefront correction system. The high-order wavefront variance caused by the temporal constraints is [29]:

$$\sigma_{temp}^2 = \left(f_G/f_{3\mathrm{dB}}\right)^{5/3}. \tag{9}$$

After substituting σ_{temp} into Eqs. (7) and (8), CE can be calculated with the effect of the bandwidth of the high-order wavefront correction system.

Assuming that the receiving fiber aperture is equal to the ideal Airy disk ($2.44\lambda f/D$), CE is calculated using Eqs. (7) and (8) to analyze the effect of the bandwidth of the high-order wavefront correction system (Fig. 2(a) and (b), respectively). As shown in Fig. 2(a), the CE is reduced from 0.82 to 0.09 when the RMS increases from 0 to 2 rad and their relation is nonlinear. When the RMS is equal to 1 rad, the CE decreases to 0.45. Therefore, the correction error of 1 rad is insufficient for FSLC. However, for astronomical applications, the RMS value of 1 rad is acceptable after adaptive correction. The requirement of AO is different for astronomy and FSLC applications. The effect of system bandwidth is shown in Fig. 2(b). The CE decreases to 0.45 when $f_G/f_{3\mathrm{dB}} = 1$ and to 0.13 when $f_G/f_{3\mathrm{dB}} = 2$. Hence, a high system bandwidth is needed for FSLC. Fig. 3 shows the effect of system bandwidth on CE at different receiving fiber apertures.

2.2. BER

Given that "zero" bit is not related to the "one" bit in the binary code (in fiber optical communication, BER is 10^{-9}), the average BER with adaptive correction may be written as [27]:

$$\langle BER\rangle = \frac{1}{2} erfc\left(\sqrt{18\cdot CE}\right), \tag{10}$$

where $erfc$ is the complementary error function:

$$erfc\,(x) = 1 - \frac{2}{\sqrt{\pi}}\int_0^x \exp\left(-z^2\right) dz. \tag{11}$$

According to Eqs. (10) and (11), after the correction, the influences of residual wavefront and $f_G/f_{3\mathrm{dB}}$ on BER are shown in Fig. 4(a) and (b), respectively. As shown in Fig. 4(a), the communication BER increases with increasing correction error. The communication BER is typically less than 10^{-6} to realize optical communication. Under the condition of the ideal communication BER of 10^{-9}, the RMS value of the correction error should be less than 0.67 rad to acquire the BER of 10^{-6}. According to the calculation results in Fig. 2, the CE should be more than 0.62. The effect of the system bandwidth is shown in Fig. 4(b). When $f_G/f_{3\mathrm{dB}} = 0.62$, the communication BER is less than 10^{-6}. Consequently, $f_{3\mathrm{dB}}$ shall be 1.6 times of f_G to achieve normal optical communication. The effect of the system bandwidth on BER is shown in Fig. 5 at different laser receiving apertures. The optimal system can be designed according to this effect.

3. Field demonstration

An outdoor experiment was performed to validate our theoretical analysis. The optical setup of the adaptive optics system (AOS) is shown in Fig. 6. Lasers of 1550 nm and 808 nm are selected as signal and beacon light, respectively, which are received by a telescope with an aperture of 150 mm and collimated by lens L1 (Fig. 6(a)). The collimated beam is reflected by a tip-tilt mirror (TTM) and a DM and goes to beam splitter P1, which is designed to reflect 80% of 808 nm beam and transmit light

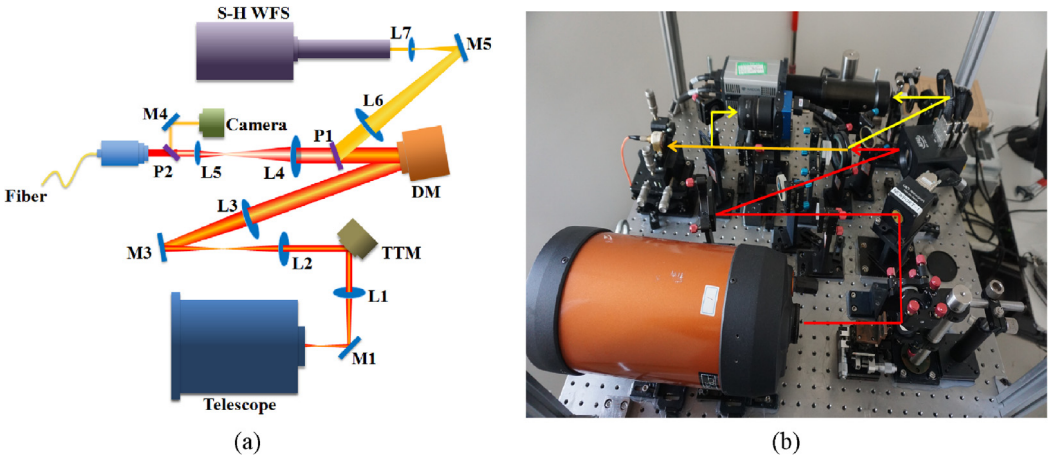

Fig. 6. AOS for FSLC: (a) designed; and (b) actual configuration.

Fig. 7. Location for the field experiment of the FSLC.

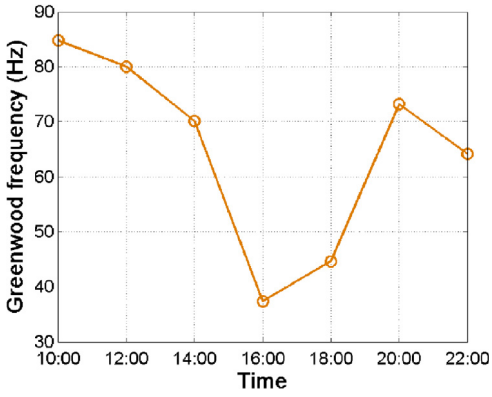

Fig. 8. Measured f_G within 12 h.

of 1550 nm and 20% of 808 nm. Thus, the light is split into two beams by P1, that is, the reflected light with the wavelength of 808 nm enters the Shack–Hartmann wavefront sensor (S–H WFS) for wavefront detection and the transmitted light is split again by P2. The transmitted 1550 nm signal light is coupled into a fiber, and the reflected light with the wavelength of 808 nm is received by a tracking camera. Fig. 6(b) shows the actual optical configuration of the designed AOS. The diameter of the fiber end face is 100 μm, which is 1.8 times that of the Airy disk. The S–H WFS has parameters of 1.6 kHz frame frequency, 15 × 15 microlenses, and 2.3 mm aperture. The DM is purchased from ALPAO and possesses 145 actuators, 4 kHz first resonance of the membrane, and 30 mm aperture. The TTM (FSM-300, Newport) with the tip-tilt angle ±1.5° and 25.4 mm aperture is used to correct tip-tilt aberrations. The tracking camera (EoSens GE, Mikrotron) is used to obtain the tracking error with an ROI area of 90 × 90 pixels and 500 Hz frame frequency. With these devices, the 3 dB bandwidth of the AOS is tested, and the value is 50 Hz.

Two stations are selected to perform the FSLC experiment with the distance of 9 km (Fig. 7). The transmitting and receiving terminals are placed at the PaoTai Mountain and MiaoXi, respectively. The signal and beacon lasers are emitted from the PaoTai Mountain with the wavelengths of 1550 nm and 808 nm. The transmitted light is received by a 150 mm telescope at MiaoXi.

The f_G of atmospheric turbulence is measured at the wavelength of 1550 nm. The f_G is recorded from 10 a.m. to 10 p.m. with an interval of 2 h, and the measured data are shown in Fig. 8. The change trend of f_G differs to that of vertical turbulence because of the effect of ground layer weather.

Laser communication is operated simultaneously with adaptive correction to evaluate the effect of the system bandwidth on the FSLC and measure f_G. To do the adaptive correction, the response matrix of DM should be measured firstly. A 808 nm laser outputted with a fiber is placed at the focus of the telescope and the response function of each actuator is measured with the S–H WFS. After this, the 808 nm laser is moved out from the AOS. The wavefront reconstruction is based on modal method and the first 18 modes of Zernike polynomial is utilized correct the high order aberrations. The tip-tilt aberration is corrected by the TTM. The RMS of the wavefronts, calculated with an average of 2000 data to acquire the statistical result, are shown in Fig. 9(a) without and with the adaptive correction. After the correction, the wavefront error is reduced from 4.3 rad to 1.1 rad with $f_G = 45$ Hz. Fig. 9(b) shows the corrected wavefront error at different $f_G/f_{3\text{dB}}$, which is obtained with the measured f_G (shown in Fig. 8) and $f_{3\text{dB}}$. The fitting result of the measured data is represented with a dashed line. For comparison, time delay error σ_{temp} is computed according to the measured f_G and $f_{3\text{dB}}$ by using Eq. (9) and is also shown with a real line. The tendency of the dashed line is similar to that of the real line. However, the difference between the dashed and real lines is 0.2 rad, which is possibly caused by the errors of detection, correction, and so on.

In adaptive correction, the CE and BER are measured, and their average values are computed with 2000 data. Fig. 10 shows the measured results of CE and BER at the communication rate of 2.5 GHz. As shown in Fig. 10(a), after the adaptive correction, the CE increases from 0.24 to 0.42, and the BER decreases from 4×10^{-3} to 6×10^{-5} with $f_G = 45$ Hz. Fig. 10(c) and (d) show the CE and BER as functions of residual wavefront error. The dot, dashed, and real lines represent the measured, fitted, and theoretical results, respectively. The fitted curve of the measured data almost coincides with the theoretical curve. Therefore, Eqs. (7) and (8) can be used to calculate the effect of residual wavefront error on CE and BER.

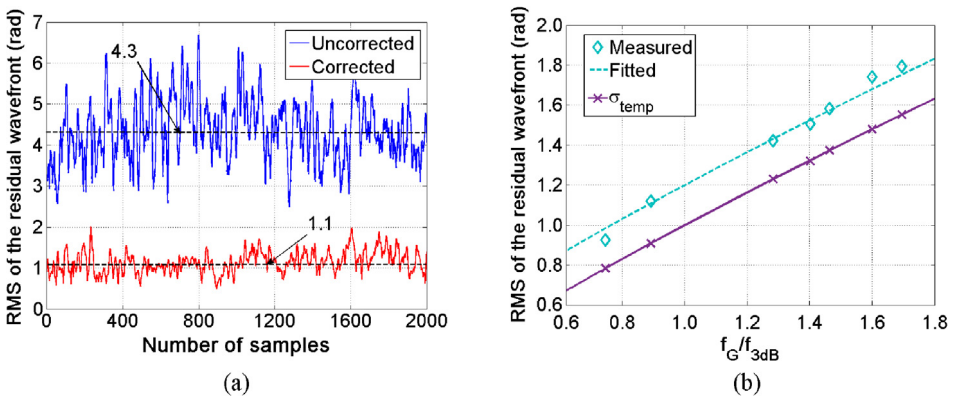

Fig. 9. Residual error with adaptive correction: (a) wavefront error before and after correction with 2000 sampling points at f_G = 45 Hz; and (b) average RMS of residual wavefront at different f_G/f_{3dB}.

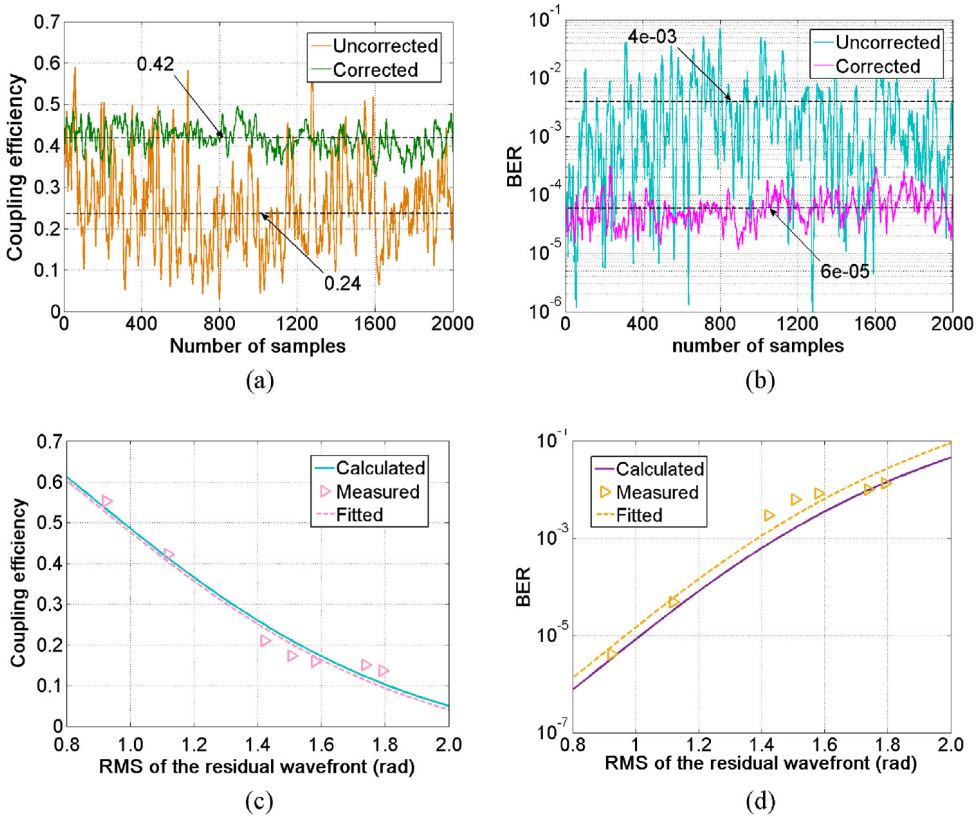

Fig. 10. Relation between CE and correction error: (a) and (b) CE and BER before and after correction with 2000 sampling points; and (c) and (d) CE and BER as functions of correction error with measured and calculated results.

The effects of f_G/f_{3dB} on the CE and BER are shown in Fig. 11(a) and (b), respectively. The real line indicates the calculated CE according to the measured σ_{temp}, and the dashed line indicates the fitting curve of the measured CE. The two curves have a difference of 0.1, which could be due to correction errors, except time delay error (Fig. 9(b)). Given that the CE only decreases 0.1, the effect of all other errors is minimal compared with that of the time delay error. Hence, in horizontal FSLC, the system bandwidth is a key factor that affects communication performance. Similar results may be obtained with regard to the effect of the system bandwidth on communication BER. All the results show that the theoretical equations can be used to analyze the effects of residual wavefront error and system bandwidth on communication performance.

4. Discussion

The RMS of all errors, except temporal error, is only 0.2 rad. Even if f_G/f_{3dB} = 0.5, σ_{tenp} is equal to 0.56 rad, which is approximately two times of all the other error. The system bandwidth of AOS considerably affects the communication performance. According to the device performances of our AOS, the 3 dB system bandwidth should be approximately 80 Hz. Given the additional time delay of 2 ms at the WFS, the measured bandwidth is only 50 Hz. The bandwidth of DM based AOS is typically 80 Hz or higher. Therefore, assuming that the system bandwidth is improved to 80 Hz, the improvements in the CE and BER are shown in Fig. 12 after the adaptive correction. When the system bandwidth is increased from 50 Hz to 80 Hz, the CE increases and the BER decreases. Under the condition of BER = 10^{-6}, the f_G of turbulence that can be overcame increases from 28 Hz to 45 Hz. The duration of optical

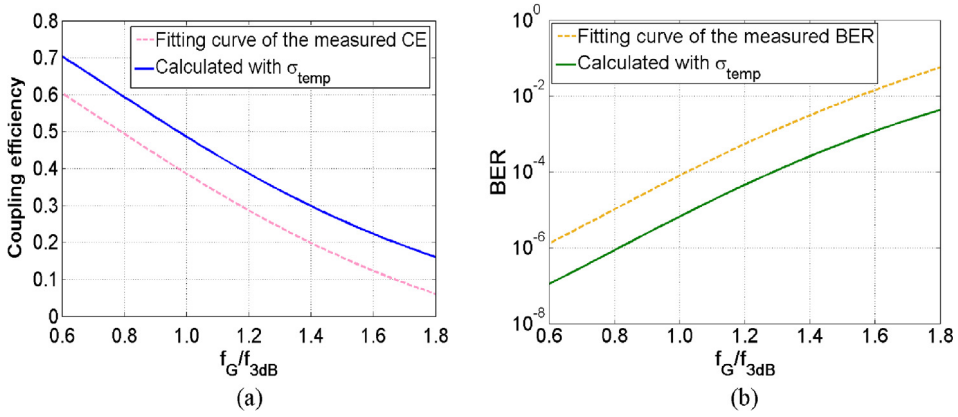

Fig. 11. (a) CE and (b) BER as functions of $f_G/f_{3\mathrm{dB}}$.

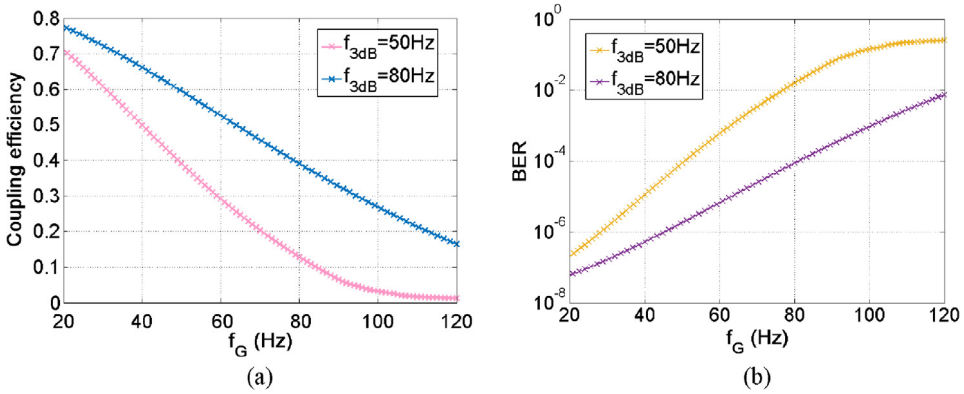

Fig. 12. (a) CE and (b) BER as functions of f_G.

communication is consequently improved. Hence, system bandwidth is a key factor that should be considered in designing AOS for FSLC.

5. Conclusions

The effect of the 3 dB bandwidth of AOS on FSLC performance is mainly studied using PIB method. A simplified model of the FSLC is established, and theoretical analysis is performed to determine the effects of temporal error. The simulation results show that the 3 dB system bandwidth should be 1.6 times of the Greenwood frequency when the fiber receiving end face is equal to the ideal Airy disk to ensure the BER of 10^{-6}.

A 9 km horizontal maritime link experiment is performed with adaptive correction to validate the theoretical analysis. The experimental results are close to the theoretical ones. Therefore, the formulas are validated for theoretical analysis of the effect of system bandwidth. Moreover, the experimental results indicate that the residual error is only 0.2 rad (except for the time delay error) after correction. Even if $f_G/f_{3\mathrm{dB}} = 0.5$, σ_{tenp} is equal to 0.56 rad. For horizontal link, the system bandwidth is a key factor that affects FSLC performance. Furthermore, with the system bandwidth is 50 Hz, f_G of 29 Hz can be overcome, and BER of 10^{-6} can be achieved. When the system bandwidth is improved to 80 Hz, the f_G of 45 Hz can be overcame. Thus, improving the system bandwidth of AOS is a major work for horizontal FSLC in the future.

The effect of the system bandwidth can be accurately evaluated with PIB method. This work provides a basis for designing and evaluating AOSs for FSLC.

Acknowledgment

This work was supported by the National Natural Science Foundation of China (Nos. 11774342, 61805238).

References

[1] W.S. Rabinovich, C.I. Moore, R. Mahon, P.G. Goetz, H.R. Burris, M.S. Ferraro, J.L. Murphy, L.M. Thomas, G.C. Gilbreath, M. Vilcheck, Free-space optical communications research and demonstrations at the U.S. Naval Research Laboratory, Appl. Opt. 54 (2015) F189.
[2] R.L. Phillips, Laser Beam Propagation through Random Media, second ed., SPIE Press, 2005.
[3] R. Lange, D. Giggenbach, 142 km, 5.625 Gbps free-space optical link based on homodyne BPSK modulation, in: Lasers and Applications in Science and Engineering, 2006, pp. 61050A-61050A-61059.
[4] A. Biswas, M.J. Novak, M. Jeganathan, 45-km horizontal-path optical link experiment, Proc. SPIE - Int. Soc. Opt. Eng. 3615 (1999).
[5] A. Belmonte, A. Rodríguez, F. Dios, A. Comerón, Phase compensation considerations on coherent free-space laser communications system in: Optics/Photonics in Security and Defence, 2007, pp. 67361A-67361A-67311.
[6] A. Belmonte, Influence of atmospheric phase compensation on optical heterodyne power measurements, Opt. Express 16 (2008) 6756.
[7] M. Cvijetic, M. Li, Coherent free space optics communications over the maritime atmosphere with use of adaptive optics for beam wavefront correction, Appl. Opt. 54 (2015) 1453.
[8] I. Toselli, S. Gladysz, Adaptive optics correction for oceanic turbulence-affected laser beams, in: Imaging and Applied Optics 2018 (3D, AO, AIO, COSI, DH, IS, LACSEA, LS & C, MATH, pcAOP), Optical Society of America, Orlando, Florida, 2018, p. JW5I.3.
[9] K. Stein, Correction of atmospheric effects on laser beams for sensing and communication, in: Imaging and Applied Optics 2018 (3D, AO, AIO, COSI, DH, IS, LACSEA, LS & C, MATH, pcAOP), Optical Society of America, Orlando, Florida, 2018, p. SM2H.1.
[10] C. Petit, N. Vedrenne, V. Michau, G. Artaud, J.L. Issler, E. Samain, M. Toyoshima, M. Akioka, D. Kolev, Y. Munemasa, Adaptive optics results with SOTA, in: IEEE International Conference on Space Optical Systems and Applications, 2016, pp. 1-7.
[11] E. Chen, Research on adaptive optics in satellite-to-ground laser communication, Proc. SPIE - Int. Soc. Opt. Eng. 8331 (2011) 3.
[12] N.H. Schwartz, N. Védrenne, V. Michau, M.T. Velluet, Mitigation of atmospheric effects by adaptive optics for free-space optical communications, in: Atmospheric Propagation of Electromagnetic Waves III 2009, pp. 72000J-72000J-72011.

[13] L. Zuo, A. Dang, Y. Ren, H. Guo, Performance of phase compensated coherent free space optical communications through non-Kolmogorov turbulence, Opt. Commun. 284 (2011) 1491–1495.
[14] W. Liu, W. Shi, J. Cao, Y. Lv, K. Yao, S. Wang, J. Wang, X. Chi, Bit error rate analysis with real-time pointing errors correction in free space optical communication systems, Optik - Int. J. Light Electron Opt. 125 (2014) 324–328.
[15] M. Chen, C. Liu, D. Rui, H. Xian, Performance verification of adaptive optics for satellite-to-ground coherent optical communications at large zenith angle, Opt. Express 26 (2018) 4230.
[16] M. Li, M. Cvijetic, Coherent free space optics communications over the maritime atmosphere with use of adaptive optics for beam wavefront correction, Appl. Opt. 54 (2015) 1453–1462.
[17] C. Liu, S. Chen, X. Li, H. Xian, Performance evaluation of adaptive optics for atmospheric coherent laser communications, Opt. Express 22 (2014) 15554–15563.
[18] L. Zuo, Y. Ren, A. Dang, H. Guo, Performance of Coherent BPSK Systems Using phase compensation and diversity techniques, in: Global Telecommunications Conference, 2010, pp. 1-5.
[19] J. H, K. D, C. L, P. Z, D. J, Z. Y, Effectiveness of adaptive optics system in satellite-to-ground coherent optical communication, Opt. Express 22 (2014) 16000.
[20] C. Liu, M. Chen, S. Chen, H. Xian, Adaptive optics for the free-space coherent optical communications, Opt. Commun. 361 (2016) 21–24.
[21] C. Liu, H. Xian, M. Chen, Experimental demonstration of single-mode fiber coupling over relatively strong turbulence with adaptive optics, Appl. Opt. 54 (2015) 8722.
[22] J. Li, Z. Zhang, J. Gao, J. Sun, W. Chen, Bandwidth of adaptive optics system in atmospheric coherent laser communication, Opt. Commun. 359 (2016) 254–260.
[23] Y. Wang, H. Xu, D. Li, W. Rui, C. Jin, X. Yin, S. Gao, Q. Mu, X. Li, Z. Cao, Performance analysis of an adaptive optics system for free-space optics communication through atmospheric turbulence, Sci. Rep. 8 (2018).
[24] A.J.E. Kaufmann, Performance limits of high-rate space-to-ground optical communications through the turbulent atmospheric channel, Proc. SPIE Int. Soc. Opt. Eng. 2381 (1995).
[25] W. Liu, K. Yao, D. Huang, X. Lin, L. Wang, Y. Lv, Performance evaluation of coherent free space optical communications with a double-stage fast-steering-mirror adaptive optics system depending on the Greenwood frequency, Opt. Express 24 (2016) 13288–13302.
[26] J. Cao, X. Zhao, W. Liu, H. Gu, Performance analysis of a coherent free space optical communication system based on experiment, Opt. Express 25 (2017) 15299.
[27] X. Yin, R. Wang, S. Wang, Y. Wang, C. Jin, Z. Cao, L. Xuan, Evaluation of the communication quality of free-space laser communication based on the power-in-the-bucket method, Appl. Opt. 57 (2018) 573–581.
[28] D.L. Fried, Statistics of a geometric representation of wavefront distortion, J. Opt. Soc. Ameri. (1917-1983) 55 (1965) 1427–1435.
[29] Francois Roddier, Adaptive Optics in Astronomy, Cambridge University Press, 1999.